Heliyon 9 (2023) e22190

Contents lists available at ScienceDirect

Heliyon

journal homepage: www.cell.com/heliyon

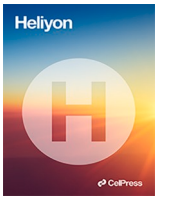

Electro-catalytic adsorption mechanism of acetonitrile in water using a ME-ACFs system

Yaping Guo [a,*], Shuo Cao [a], Sizhou Cheng [b], Xinhua Huang [a], Mengyao Ren [a]

[a] College of Environment, Zhejiang University of Technology, Hangzhou 310014, China
[b] Zhejiang Lianwei Environment Co., Ltd, China

ARTICLE INFO

Keywords:
Micro-electro-active carbon fiber coupling system
Adsorption
Acetonitrile
Electro-catalytic hydrolysis
Electro-enhanced adsorption

ABSTRACT

Acetonitrile wastewater is difficult to treat due to its high salinity and toxicity to microorganisms. In this paper, a micro electro-activated carbon fiber coupled system (ME-ACF) was established to treat simulated acetonitrile wastewater. In the 200 ml system, the concentration of acetonitrile adsorbed by ACF was 91.3 mg/L, while that of acetonitrile adsorbed by ME-ACF was 150.6 mg/L, and the removal efficiency was increased by 65 % in comparison. The activated carbon fibers before and after the reaction were subjected to a series of characterization, and it was found that the SABET decreased from 1393.48 m^2/g to 1114.93 m^2/g and 900.23 m^2/g, respectively, but the oxygen on the surface of the activated carbon fibers was increased, and the effect of the micro electrolytic system on the activated carbon fibers was then analyzed. The possible reasons for the formation of acetic acid contained in the products were also discussed using DFT simulations. The removal mechanism of acetonitrile by ME-ACF was considered to be electrically enhanced adsorption and electro-catalytic hydrolysis.

1. Introduction

Activated carbon fiber has numerous applications in the fields of energy and the environment. It is a porous fibrous material with a diameter of 5–10 μm and usually takes the form of activated carbon fiber mats in various weaves [1]. Activated carbon fibers are favored due to their high specific surface area and numerous micropores, resulting in faster adsorption rates and ease of desorption.

Initially, activated carbon fibers were produced from petroleum products [2], resulting in considerable energy consumption and the inadvertent generation of environmentally unfriendly substances. The utilization of phenolic resins [3], PAN [4], and even natural plant fibers like betel nut [5], cotton [6], and bamboo fibers [7], subsequently improved the production process of ACF. Consequently, there was a significant increase in the specific surface area of the activated carbon fibers, resulting in excellent results in the purification of pollutants and energy storage applications [8–11].

Activated carbon fibers are extensively utilized in the environmental sector for the elimination of organic matter or metallic elements from water. The recent studies have made significant advancements in the development of activated carbon fibers. A variety of activators are used to alter the surface morphology or functional groups of activated carbon fibers for improved adsorption [12,13]. Activated carbon is employed as a substrate for the attachment of organic polymers for modification or catalysts. For instance, chitosan was affixed to activated carbon fibers to improve the capture of Pb-EDTA [14], while $CuFe_2O_4$ was attached to the surface of activated

* Corresponding author.
E-mail addresses: luckyyaping@zjut.edu.cn (Y. Guo), 2112127010@zjut.edu.cn (S. Cao), 17858150275@163.com (S. Cheng), 221122270222@zjut.edu.cn (X. Huang), 211122270041@zjut.edu.cn (M. Ren).

https://doi.org/10.1016/j.heliyon.2023.e22190
Received 21 July 2023; Received in revised form 5 November 2023; Accepted 6 November 2023
Available online 13 November 2023

carbon to boost oxidative degradation of phenol [15],and titanium dioxide was attached to activated carbon fibers for toluene degradation [16]. Certain potentials were deployed to enhance the adsorption capacity of activated carbon fibers. For example, alginate-activated carbon was treated with a certain potential to tackle phenol wastewater [17]. Recent studies have mainly focused on aeration biofilm as a means of acetonitrile wastewater treatment, while the literature on activated carbon adsorption is limited [18–21].

As early as 2008 Cai et al. [22] conducted adsorption experiments using commercial activated carbon as well as two types of commercial activated carbon fibers and the result was that the activated carbon fibers were more effective, but no explanation was given for this other than the higher specific surface area of the activated carbon. Regarding the electro sorption of organic substances, K.Y. Foo et al. [23] gave a summary that the adsorption performance depends on the surface functional groups as well as the magnitude of the polarity of the substance. Later, Sylwester Furmaniak et al. [24] verified and concluded that changing the polarity of functional groups is more effective in adsorbing the target substance than increasing the porosity. Urita et al. [25] compared the adsorption of acetonitrile and water on activated carbon fibers under a certain pressure and concluded that pore adsorption and binding of oxygen-containing functional groups are simultaneous processes in adsorption of acetonitrile on activated carbon. Zhou et al. [26] proposed a method for the removal of polar organic matter from water by electrodeposition activated carbon and provided some experimental basis for the regeneration of activated carbon fibers.

In this study, activated carbon fiber mats were affixed onto platinum sheets to induce a consistent potential and enhance the adsorption capability of activated carbon. Acetonitrile, known to be a Lewis base, can be captured more effectively through oxidation of activated carbon in the presence of an electric current. This results in an increase in the proportion of surface functional groups containing oxygen, which in turn bonds with acetonitrile. The ME-ACF system employed in this study therefore demonstrates superior performance compared to ACF. The reason we use platinum as an electrode is that acetonitrile is able to undergo a hydrolysis reaction on the surface of the platinum electrode., the reason for this will be given later.

2. Materials and methods

2.1. Materials

Acetonitrile (HPLC), activated carbon fiber, Pt electrode, saturated calomel electrode, deionized water, electrolytic cell , acetyl acetamide, hexane sulfonic acid et al.

Before use, the activated carbon fibers are soaked and shaken in deionized water for 4 h, rinsed repeatedly and finally dried in a vacuum oven at 120 °C for up to 12 h.

2.2. Physical characterization and gas sorption measurement of ACFs

The specific surface area was determined using an automated physical adsorbent apparatus (ASAP 2460) and BET calculations, and the micropore volume was evaluated. The surface morphology of ACF at different scales was observed using a field emission scanning electron microscope (S-4800). X-ray diffraction (XRD) patterns of ACF were obtained using an X-ray diffractometer (ARL X'TRA Companion) with Cu KR as the radiation source. Raman spectra were obtained using a Raman spectrometer (Lab RAM HR Evolution) with a 532 nm excitation laser. X-ray photoelectron spectroscopy (XPS) was determined using a K-Alpha + photoelectron spectrometer (Thermo) to determine the amount of elemental C, N, O on the surface of ACF before and after the reaction, and thus to infer the changes in the functional groups on the surface of ACF before and after the reaction.

2.3. Adsorption performance evaluation

0.1g of samples were added to a reactor containing 200 mL of a 200 mg/L acetonitrile solution. The mixture was shaken in a water bath shaker at 300 rpm for 30 min. The concentration of acetonitrile was determined by GC (Agilent 7890A) after filtering through a 0.45 μm filter. The acetonitrile adsorption capacity was calculated using the following equation:

$$q=((C_0–C) \times V)/m \quad \text{(Formula 1)}$$

where q is the adsorption capacity (mg/g), C_0 and C represent the initial and final acetonitrile concentrations (mg/L), V (L) represents the volume of the acetonitrile solution, and m represents the mass of the adsorbent (g).

2.4. ME-ACF and ACF adsorption experiment

ME-ACF: Platinum electrodes (2 × 2 × 0.2 cm) of anode and cathode were uniformly wrapped with 0.2 g of activated carbon fiber and fixed with electrode clips. Next, the electrodes were placed in a solution containing 200 mg/L acetonitrile and 10 g/L sodium sulfate, and a constant voltage of −900 V was applied for 48 h. The residual acetonitrile concentration in the water was measured at regular intervals during this period.

ACF: The platinum electrodes (2 × 2 × 0.2 cm) of the anode and cathode were uniformly wrapped with 0.2 g of activated carbon fiber and fixed with electrode clips. Next, the electrodes were placed in a solution containing 200 mg/L acetonitrile and 10 g/L sodium sulfate for 48 h. During this period, the concentration of acetonitrile remaining in the water was measured regularly.

The above data were summarized, and adsorption isotherms were fitted.

2.5. Cyclic voltammetry

A platinum electrode was used as the working and auxiliary electrodes, and a saturated calomel electrode was used as the reference electrode to determine the cyclic voltammetry curve of 200 mg/L of electrolyte-containing acetonitrile solution. The voltage range was set at −1.0V–1.0V, the scan speed was 10 mV/s, and the sample interval was 1 mV. The scanning segment was scanned twice in the positive electrode direction.

2.6. Electrochemical experiments and determination of related products

Single and double chamber electrolytic cells were set up and electrochemical experiments were performed at −900 mV and 600 mV (vs. SCE), 30 ± 0.5 °C, stirring solution speed of 300 r/min, with platinum sheets as cathode and anode, and solutions containing 200 mg/L acetonitrile and 10 g/L sodium sulfate, to confirm the formation of acetic acid and to rationally explain it in conjunction with other characterization means.

The UV spectrophotometric method was used to determine the ammoniacal nitrogen and nitrate nitrogen, the infrared spectrum and gas chromatography were used to determine the acetonitrile and its degradation products, and the pH was measured using a pH electrode (PB-10).

In addition, HPLC was used to determine acetyl acetamide by using a C-18 chromatographic column with detection at a wavelength of 200 nm. The ratio of the flow phase was a mixture of 30 mM phosphate buffer and 5 mM hexane sulfonic acid (HSA) with the pH adjusted to 2.6 using phosphoric acid. The column temperature was controlled at 35 °C, and the flow rate was 0.35 mL/min [27].

The products were determined using GC-MS to obtain the spectra of acetic acid.

3. Results and discussion

As can be seen from Fig. 1(a–b), ACF has many indentations on the surface, which are overall more uniform, with neat cross sections and random pore size distribution. The pores of ACF-Cathode show no significant change, but the fibers of this sample show jagged cross-sections, and the surface grooves are deepened in comparison to that of ACF, Fig. 1(c–d). Fig. 1(e–f), whereas ACF-Anode showed more cross sections as well as fiber fragments and wider and deeper notches on the activated carbon fibers.

The BET analysis leads to Table 1. From the table applying constant voltage to ACF, its SABET decreases significantly from 1393.48 m^2/g to 1114.93 m^2/g or even 900.23 m^2/g. N_2 adsorption analyses were carried out on ACF, ACF-Cathode and ACF-Anode to obtain the porosity.

As seen in Fig. 2(a–c) the samples all show a sharp increase in N_2 absorption in the low-pressure region ($P/P_0 > 0.01$), indicating a high degree of microporosity. In addition, Fig. 2(d–f), there is a trend for all samples to rise between 300 and 400 mmHg, consistent with a combination of Type I and Type IV(b) adsorption isotherms, and the rise is greater for Sample ACF, so there is a greater proportion of mesopores in this sample. Samples ACF-Cathode and ACF-Anode in which the proportion of mesopores is less is due to the oxidation-induced fracture of the activated carbon fibers, which results in a large loss of specific surface area and pore volume. In addition, the oxidation of the electric current forms a large number of oxygen-containing functional groups on the pore surfaces of the

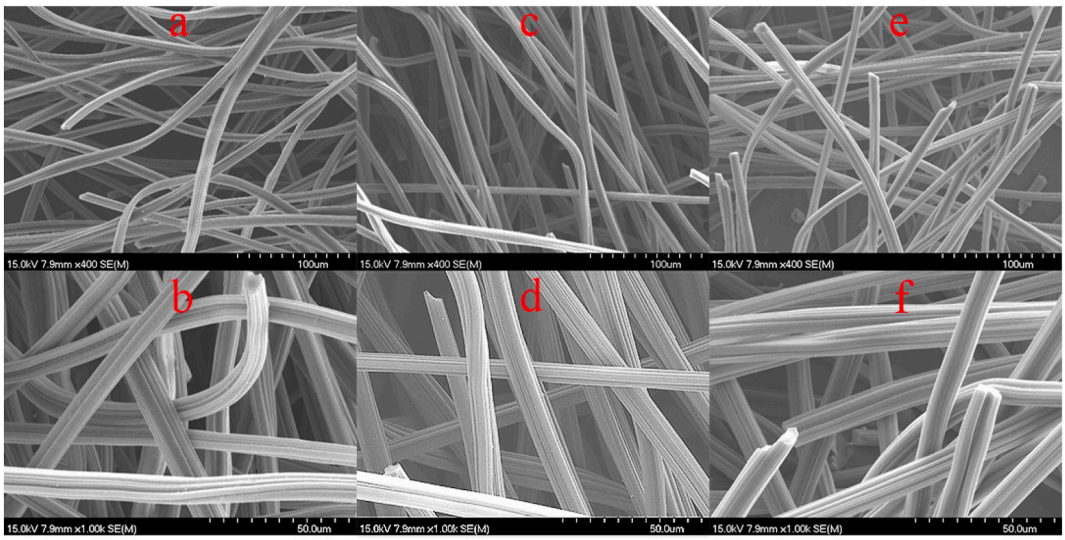

Fig. 1. SEM images of (a–b) ACF, (c–d) ACF-Cathode and (e–f) ACF-Anode.

Table 1
Textural properties of ACF, ACF- Cathode and ACF-Anode derived using N_2 sorption isotherm measured at 77 K.

Sample	SA_{BET} (m^2/g)	Pore size (nm)	Pore volume (cm^3/g) @ 0.95(p/p_0)
ACF	1393.48	1.79 , 3.15	0.62
ACF- Cathode	1114.92	1.77 , 3.01	0.49
ACF- Anode	900.23	1.76 , 2.89	0.40

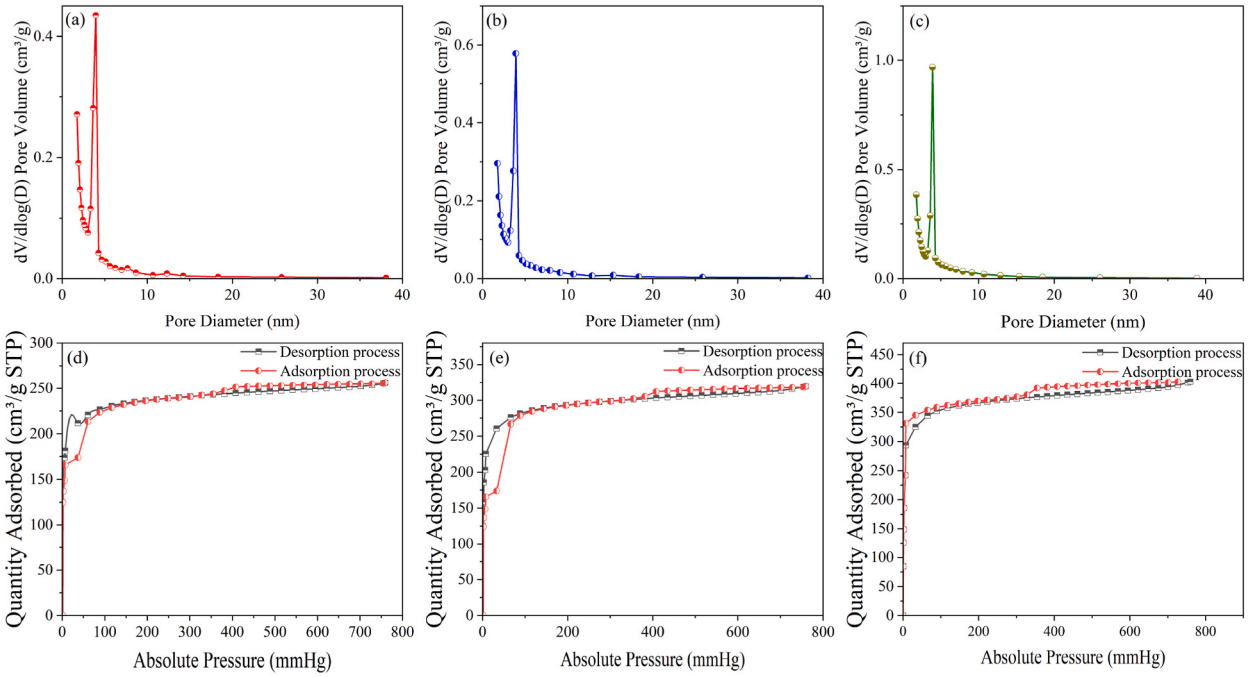

Fig. 2. N_2 sorption study; (a–c) pore size distribution and (d–f) N_2 isotherms of ACF, ACF-Cathode and ACF-Anode.

internal pores of the activated carbon, which adsorb on the inner surface of the pores, resulting in the narrowing of the pores, and therefore the reduction of the specific surface area and pore volume. At the same time, the appearance of some sections also led to the formation of a small number of micropores inside the activated carbon. An increase in pore volume was also observed at a P/P0 of 0.95, with corresponding values of 0.40 cc/g, 0.49 cc/g and 0.62 cc/g for the samples.

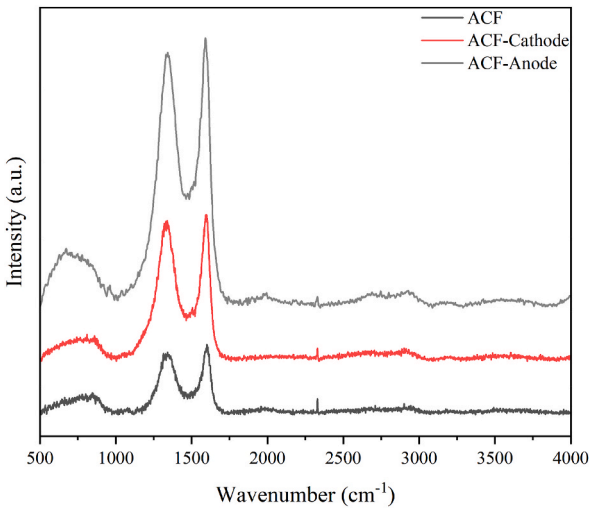

Fig. 3. Raman spectra of ACF, ACF-Cathode and ACF- Anode.

As shown in the Raman spectra included in Fig. 3, there are obvious D bands and G bands, the D band at 1340 cm^{-1} can be attributed to the defects and disordered arrangement of the carbon crystals, while the G band at 1580 cm^{-1} is due to the sp2 stretching vibration of the C element.

The I_D/I_G values of the three samples in the figure are 0.837, 0.838, and 0.840, respectively, which are used to judge the degree of ordering. The final results show that the carbon fiber defects in ACF-Anode are slightly smaller than those in ACF, and it is presumed that there is a partial oxidation fracture of C═C in it.

The XRD patterns of ACF-Anode and ACF-Cathode were also measured and compared with the XRD patterns of the initial ACF. Fig. 4 shows that the carbon on the surface of ACF is all amorphous and therefore broad peaks appear at 2θ of 23–28° and 41–45°. Combined with the SEM images and the results of BET, it can be concluded that the amorphous carbon content inside ACF increases under constant potential, and the associated oxygen-containing functional groups also increase.

The elemental composition and chemical nature of ACF- Cathode and ACF- Anode were analyzed by XPS. The scan shown in Fig. 5 confirms the presence of small amounts of elemental S and Na in the activated carbon, indicating that there is a small amount of sodium sulfate residue in the activated carbon fibers, therefore washing the sample with water alone is not sufficient to remove the inorganic salts contained in the sample, and washing with acid should be given due consideration. The elemental composition of ACF is 20.35 (O),73.77(C),5.88(N). The elemental composition of ACF-Cathode is 35.93(O),46.39(C),3.91(N),8.33(Na)5.44(S). The elemental composition of ACF-Anode is 22.87(O),71.27(C),5.00(N),0.65(Na)0.2(S).

High-resolution C1s XPS spectra indicate that ACF-Cathode consists of four different types of carbon: sp2 C, sp3 C, C–O/C═N, and pyrolytic acid, 284.8, 285.2, 285.7, and 286.8 eV, respectively, Fig. 5(a). High-resolution XPS spectra of the O1 and N1s indicate that there are two types of oxygen present in ACF-Anode (C -O; 532.1 eV and C═O; 533.5 eV), Fig. 5(b), and three types of nitrogen (pyridine nitrogen; 399.1 eV, pyrrole nitrogen; 400.6 eV and graphite nitrogen; 402.5 eV), Fig. 5 (c).

In addition, from Fig. 5. (d), the C1s of ACF-Anode possesses four different types of carbon, and these carbon peaks are present at 283.86 eV, 284.80 eV, 285.57 eV, and 27.55 eV, which corresponds to sp2C, sp3C, C–O/C═N vs. C═O. The high-resolution XPS spectra of the O1s show two peaks at 531.24 and 535.32 eV which correspond to sp2C, sp3C, C–O/C═N vs. C═O. The high resolution XPS spectra of the O1s show two peaks at 531.24 and 535.32 eV which corresponds to sp2C, sp3C, and C═O. The two peaks at 531.24 and 535.32 eV correspond to C–O and C═O functional groups, see Fig. 5(e). The N1s high-resolution XPS spectra consisted of three peaks due to the confirmation of the presence of pyridinium nitrogen, pyrrole nitrogen, and graphitic nitrogen observed at 398.39, 399.4, and 400.00 eV, respectively, see Fig. 5(f).

The results showed that the oxygen element in ACF increased significantly after applying a constant voltage, with the higher oxygen element in ACF-Cathode. It is presumed that the ACF-Cathode adsorbed a large amount of inorganic sulfate, which in turn increased the percentage of oxygen elements. The oxygen element in ACF-Cathode is mostly increased in the form of C═O/C–O, which is easier to be combined with acetonitrile, a Lewis basic substance.

3.1. Kinetics and adsorption isotherm analysis

The adsorption data were fitted as shown in Fig. 6, and from the results of adsorption isotherms, it is clear that the micro electrical system promotes the adsorption performance of the activated carbon fibers. The Langmuir model fits the data better, and the correlation ($R^2 = 0.87$) is clearly higher than that of the Freundlich model ($R^2 = 0.80$), which suggests that the process of adsorption of acetonitrile by ME-ACF consists mainly of a monolayer of chemisorption, Fig. 6. (a,b). Specific values for the adsorption simulations can be found in Table 2. However, the experimental data were not fully consistent with the adsorption mechanism, so it was speculated

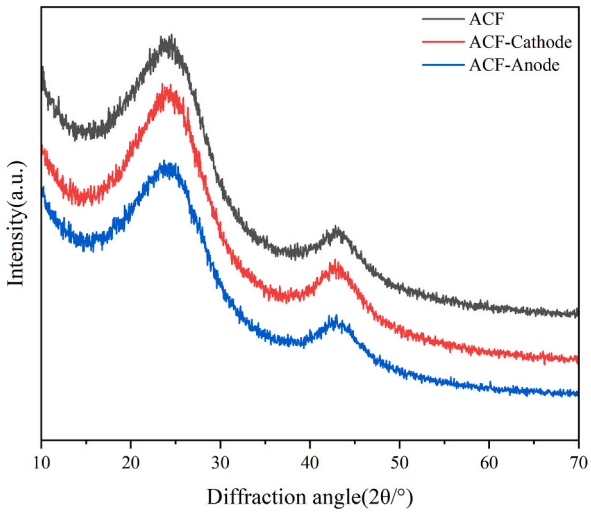

Fig. 4. XRD patterns of ACF, ACF-Cathode and ACF-Anode.

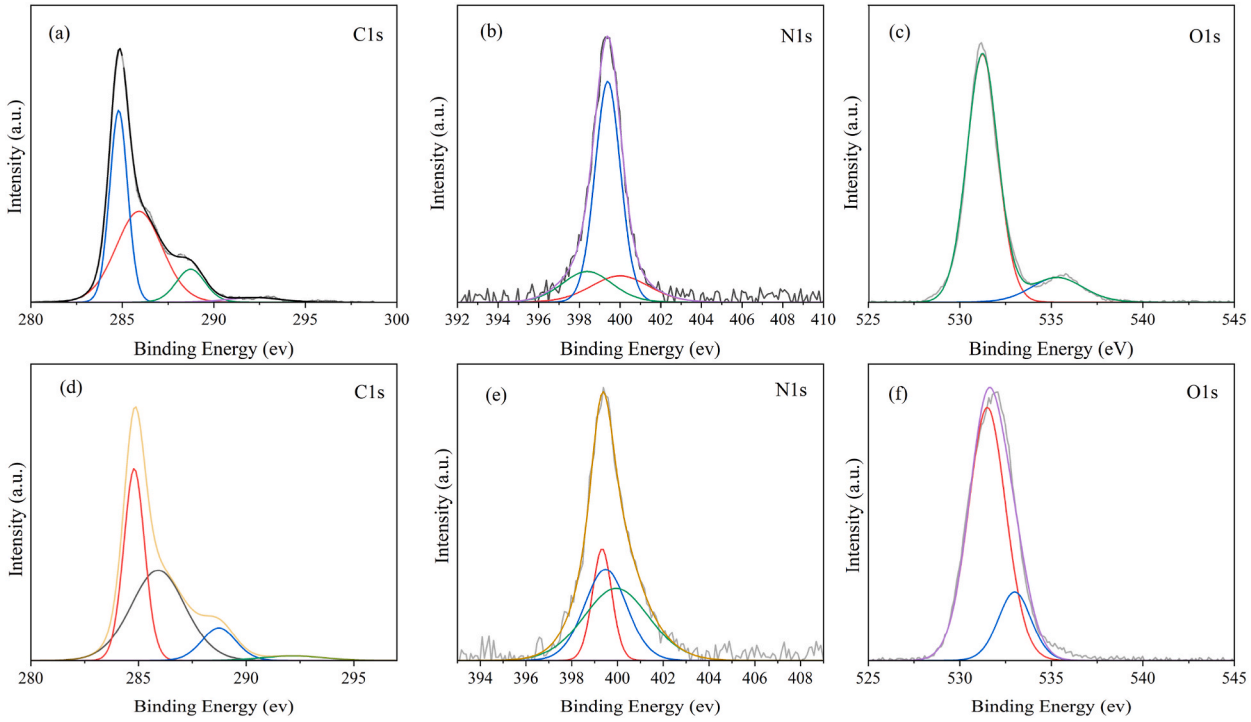

Fig. 5. XPS spectra; for ACF-Cathode (a) C1s, (b) O1s and (c) N1s, and for ACF-Anode (d) C1s, (e) O1s and (f) N1s.

that acetonitrile might have undergone a chemical reaction. In addition, the pseudo-first order model well described the adsorption behavior of acetonitrile by ACF and ME-ACF, Fig. 6 c, but the better adsorption effect of ME-ACF ($R^2 = 0.9738$) than that of ACF ($R^2 = 0.9748$) suggested that the action about micro electricity on activated carbon fiber or acetonitrile in ME-ACF might be the rate-limiting step for acetonitrile adsorption. The pseudo-first order fit showed that the removal efficiency of ME-ACF was consistently higher than that of activated carbon fiber adsorption alone after 6 h of adsorption. During the first 6 h, the rate of acetonitrile diffusion from the solution to the adsorbent surface decreased significantly and gradually equilibrated, which can be attributed to the saturation of acetonitrile adsorption by micropores as well as mesopores in the activated carbon fibers. And the kinetic simulation of this experiment can be shown by Fig. 6(d).

$\boldsymbol{C_e}$: equilibrium concentration of acetonitrile (mg/L) ; $\boldsymbol{Q_e}$: equilibrium adsorption capacity of acetonitrile (mg/g) ; $\boldsymbol{Q_m}$: maximum unit adsorption capacity of acetonitrile (mg/g) ; $\mathbf{K_L}$: Langmuir constant; $\boldsymbol{K_f}$: Freundlich constant; $\frac{1}{n}$: adsorption index;

According to the information provided by the manufacturer, activated carbon fibers mainly contains functional groups such as hydroxyl, carboxyl, and carbonyl. The pH value of AC was measured to be 5.87 ± 0.03. The experimental data calculated the adsorption capacity of this type of AC fiber to be 0.455 mg g^{-1}.

According to Marc T.M. Koper et al. it is shown that at electrode potentials higher than 0.55 V, adsorbed OH(OH_{ad}) is reversibly formed on the surface of Pt (1,1,1) (Formula 2) [28].

$$(Pt + H_2O \rightleftharpoons Pt\cdots OH + H^+ + e^-) \qquad \text{Formula 2}$$

whereas at potentials lower than 0.35 V, hydrogen is adsorbed on the surface of Pt (1,1,1). (Formula 3) [29].

$$(H_3O^+ + e^- + Pt \rightleftharpoons Pt\cdots H + H_2O.) \qquad \text{Formula 3}$$

As shown in Fig. 7, no significant differences are observed in the cyclic voltammetry (CV) curves between the sodium sulfate solution (Fig. 7. (a)) and the acetonitrile solution supplemented with sodium sulfate (Fig. 7. (b)). Therefore, we can conclude that there has been no direct occurrence of oxidation or reduction reactions.

Additionally, the cyclic voltammetry curve obtained from the experiment showed a clear reduction peak at −0.9V. An oxidation peak exists at −0. 5~0V. This oxidation peak is believed to be generated by the hydrogen desorption process on the platinum electrode and at 0.3~3V, sulfate resolution occurs on the platinum surface and the cyanide on acetonitrile bonds to the platinum atoms blocking the other adsorption sites [30]. It is thus demonstrated that the anode can still adsorb a certain amount of acetonitrile when −900 mV is applied, while the cathode can adsorb sulfate to prevent effects on the adsorbed acetonitrile.

After a certain duration, we observed the formation of minuscule gas bubbles in close proximity to the electrode. Hence, we deduce that the reaction mentioned below has taken place.

$$2H_2O + 2e^- = H_2 + 2OH^- \qquad \text{(Formula 4)}$$

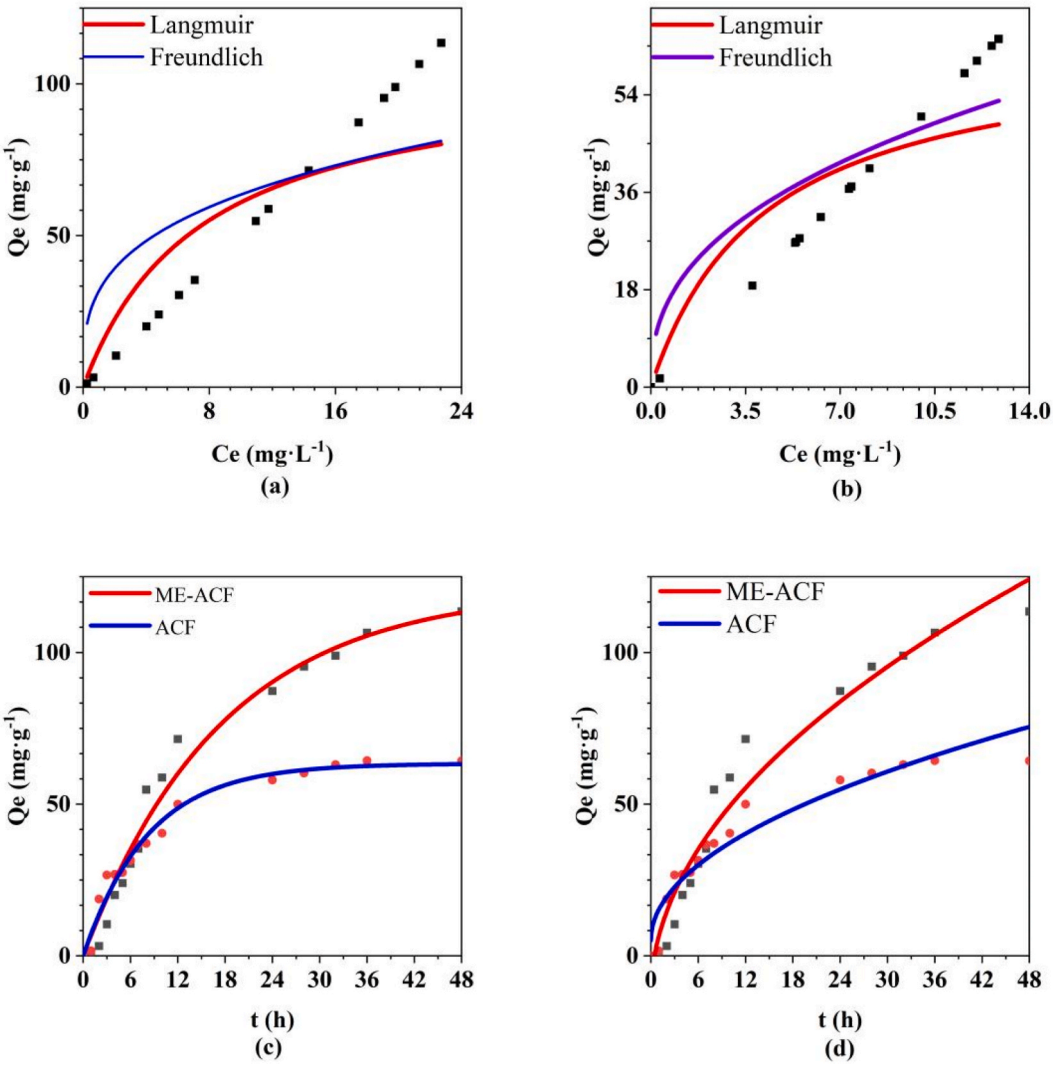

Fig. 6. Adsorption kinetics of Acetonitrile by ME-ACF (a) and ACF (b), Fitting results of pseudo-first order (c), and intraparticle diffusion (d) kinetic models.

Table 2
Adsorption isotherm parameters 30 °C.

Adsorption type	Langmuir $Q_e = K_L Q_m C_e/(1+Ce)$			Freundlich $Q_e = K_f C_e 1/n$		
	K_L	Q_m	R2	K_f	n	R2
ME-ACF	0.134 ± 0.03	106.57	0.80	31.83 ± 3.01	3.3	0.66
ACF	0.24 ± 0.05	64.34	0.87	19.04 ± 1.08	2.5	0.75

It is well known that acetonitrile contains a methyl group and a cyano group, Fig. 8, in which the cyano group belongs to the nucleophilic group, so acetonitrile is more easily adsorbed by the anode. Therefore, after acetonitrile was adsorbed onto the surface of the platinum electrode under the condition of constant −900mV, the ions generated by the ionization of water on the electrode surface were occupied by acetonitrile at the adsorption sites on the electrode surface, and thus desorbed to release hydrogen and hydroxyl. Under the catalytic effect of the two, acetonitrile is gradually hydrolyzed and detached from the electrode surface, Fig. 9. The empty adsorption sites will be occupied again by the ionization products of water molecules or acetonitrile. Since OH (OHad) is mainly adsorbed on the electrode surface and more hydroxide is desorbed when the potential is greater than 0.55 V, the hydroxide catalyzed acetonitrile hydrolysis occupies the main part, so the hydroxide catalyzed acetonitrile hydrolysis process was simulated using DFT.

The products after the single-chamber reactor experiment were analyzed using the Nessler reagent spectrophotometric method, which showed that applying microcurrents can increase the ammonia-nitrogen content in the solution. The pH values were measured,

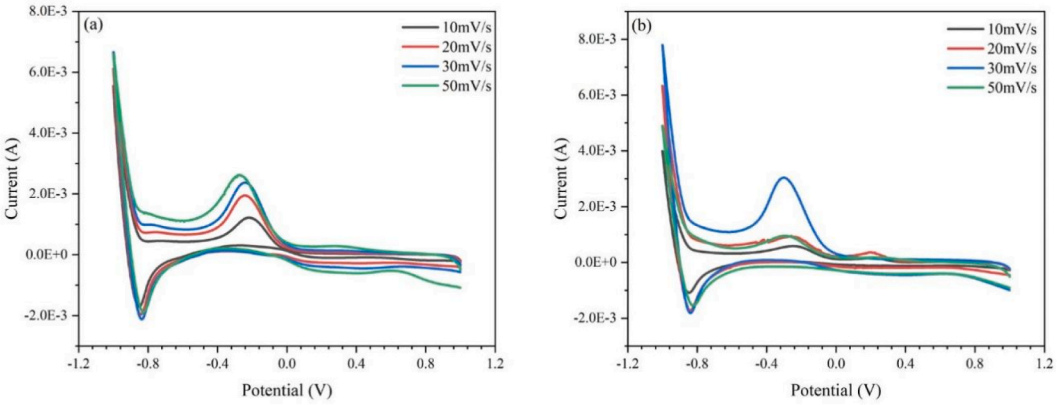

Fig. 7. Voltammetry curves of sodium sulfate (a) and acetonitrile (b).

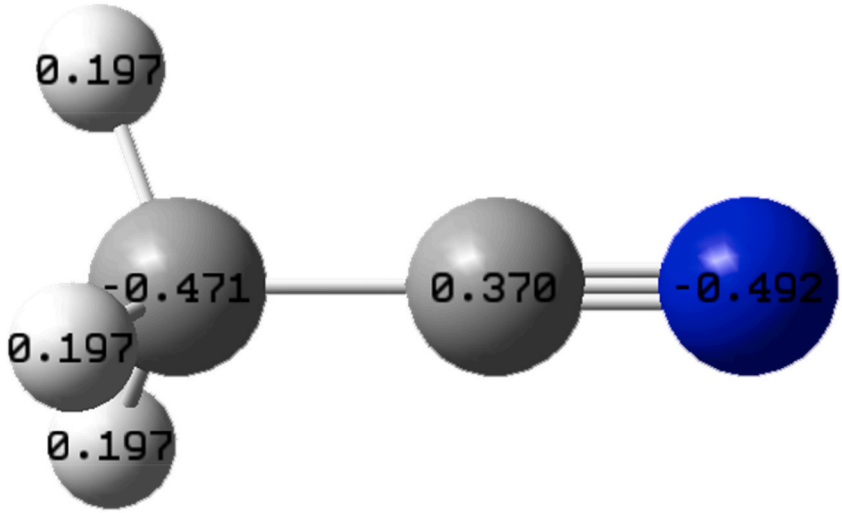

Fig. 8. Mulliken charge distribution map of acetonitrile.

and the results are as follows: pH was 6.92 at 0 h, 6.02 at 12 h, 5.46 at 24 h, and 5.43 at 48 h. The pH gradually decreased during the entire reaction process, suggesting the generation of acidic substances. The pH change was most evident in the first 24 h and then remained relatively constant. Gas chromatography measurements revealed trace amounts of acetic acid in the product, as well as a greater decrease in acetonitrile concentration than in the control group. In the two-chamber cell, when a constant current of 600 mV was applied, the concentration of acetonitrile in the chamber with the auxiliary electrode was lower than that in the chamber with the working electrode. When a constant current of −900mV was applied, the concentration of acetonitrile in the chamber with the working electrode decreased even further. The electrode pH values measured are presented in Table 3.

The pH value changed rapidly within the first 24 h and remained stable thereafter. Since there is a cation-exchange membrane between the two chambers, the difference in pH values between the two chambers is not significant. According to the ultraviolet spectrophotometric method, the concentrations of ammonia nitrogen and nitrate nitrogen in reactor A and B are shown in the table below.

From Table 4, it can be seen that the concentration of ammonia nitrogen at the working electrode is lower than that at the auxiliary electrode, while the concentration of nitrate nitrogen is the opposite. Therefore, it is speculated that ammonia nitrogen is adsorbed by the auxiliary electrode and then oxidized to nitrate nitrogen.

3.2. Calculation explanation

These structures of reactants, products and reaction intermediates were optimized under the framework of density of functional theory (DFT) with B3LYP functional [31] and 6–31++G (d,p) [32] basis set. The transition states of all possible reaction routes were also searched using the same functional and basis set. The vibrational frequency analysis was carried out for the optimized structure with the same calculation method. In order to describe the solvation effect of water, the SMD (Solvation Model Based on Density) [33]

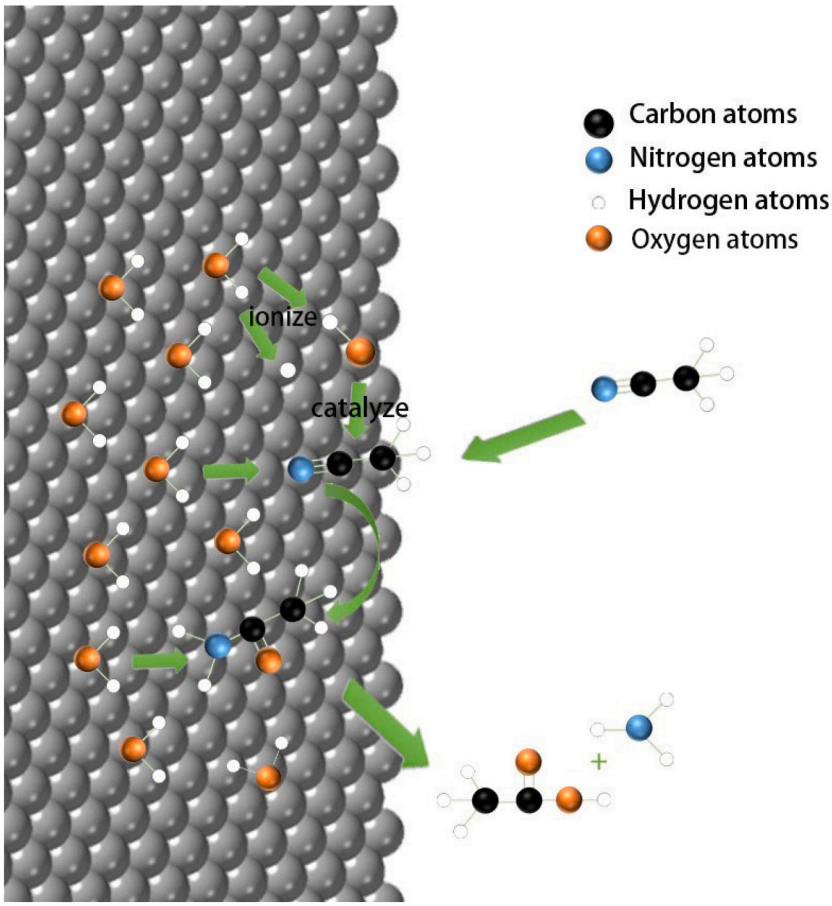

Fig. 9. Schematic diagram of the electrocatalytic hydrolysis of acetonitrile on the electrode surface.

Table 3
Electrode pH under −900 mV conditions in a double-cell electrolysis cell.

Reaction time	Working electrode pH	Auxiliary electrode pH
0	6.43	6.43
4	4.65	4.38
8	4.26	4.33
12	4.19	4.31
24	4.14	4.12
28	4.09	4.11
32	4.08	4.11
36	4.06	4.10
48	4.06	4.10

Table 4
Ammonia nitrogen and nitrate nitrogen concentrations in reactor A and B under −900 mV voltage.

	Cathode	Anode
Ammonia nitrogen concentration (mg/L)	0.053	0.166
Nitrate nitrogen concentration (mg/L)	0.335	0.692

implicit solvent model was used in all calculations. All these DFT calculations were performed using Gaussian 16 program suite [34].

Hydroxide catalyzed hydrolysis reaction pathway of acetonitrile undergoes hydrolysis reaction catalyzed by hydroxide ions, and the optimized models of its various stationary points at the B3LYP/6–31++(d,p) level in the liquid phase (water) are shown in Fig. 10. As can be seen from Fig. 10, this reaction is completed in three steps. First, the reaction complex TS1 is formed, in which one acetonitrile molecule and one water molecule combine under the action of hydroxide ions. Hydroxide ions bind to the carbon atom of

the cyanide group in acetonitrile, and the water molecule breaks an O–H bond to generate a hydroxide ion and a hydrogen ion. The hydrogen ion binds with the nitrogen atom in the acetonitrile molecule to form the first intermediate (Int1). The first intermediate exchanges a hydrogen atom with another water molecule to form the second intermediate (Int2). In this process, the intermediate breaks an O–H bond and the hydrogen atom is transferred to the water molecule. Meanwhile, the water molecule breaks an O–H bond and binds with the nitrogen atom of the second intermediate to form acetamide.

This figure mainly describes the possible steps in which acetonitrile is hydrolyzed to acetylamine and further hydrolyzed to ammonium acetate under the catalytic conditions of hydroxide ions. TS stands for transition state; Int for intermediate.

The second intermediate has an acetamide structure, and therefore can undergo further hydrolysis. For this purpose, a water molecule and a hydroxide ion are introduced into the second intermediate. The oxygen atom of the hydroxide ion binds to the carbon atom of the cyanide group in acetonitrile to form the third intermediate (Int3). In the third intermediate, the water molecule breaks an O–H bond to form a hydroxide ion, while the hydrogen ion binds to the amino group, and the C–N bond is broken, thereby generating ammonia gas and acetic acid. The reference data for the calculations can be found in Table 5.

3.3. Energy analysis

First, assuming that the free energy ΔG of the reactant acetonitrile is 0 kcal/mol, the free energy of the transition state TS1 is 27.8 kcal/mol, and the activation energy barrier between the two is 27.8 kcal/mol. In the second step, the free energy of TS2 is 19.7 kcal/mol. The activation energy barrier of this step is 11.1 kcal/mol, which is lower than the first step. Therefore, the second step is easier than the first step. Since the energy of the second intermediate is the lowest, acetamide is relatively stable and more easily formed. Similarly, the process of transformation to TS3 requires an energy barrier as high as 30.6 kcal/mol, indicating that the reaction between acetamide and a water molecule is more difficult under alkaline conditions. By comparing the activation energy barriers, we know that the third step is the rate-limiting step because its activation energy barrier is the highest. Overall, the reaction from acetonitrile to ammonium acetate requires a total activation energy barrier of −0.8 kcal/mol, which is an exothermic reaction.

To verify whether acetonitrile is hydrolyzed into acetamide product, infrared spectroscopy and GC-MS was performed, and the obtained spectrum is shown below. From Fig. 11, it can be seen that after the reaction of acetonitrile, the intensity of the absorption peak of C ≡N at the wavelength of 2248 cmˆ-1 significantly decreases. At the same time, the stretching vibration peaks at the wavelengths of 3500-3100 cmˆ-1 and 1418 cmˆ-1 can be attributed to the vibrations of N–H and C–N, indicating the generation of amide substances. In addition, the absorption peak at the wavelength of 1715 cmˆ-1 is the C═O absorption peak, and the C–O stretching vibration peak at the wavelengths of 1320-1210 cmˆ-1 indicates further hydrolysis of the amide to form a carboxylic acid. Therefore, it is inferred that the product contains acetamide and acetic acid. The infrared spectrum indirectly verifies the computational results and provides experimental support, Fig. 12.

In addition, the results showed that there was a weak hydrolysis of acetonitrile in solution state, which was about 2.8 mg. After applying a voltage of −800 mV, the concentration of acetamide in the solution adsorbed by activated carbon was about 4.3 mg after 48 h. This result also supports that the electrode produces hydroxide root which catalyzes the hydrolysis of acetonitrile.

4. Conclusion

The ME-ACF constructed in this paper showed a large advantage over the ACF in treating acetonitrile wastewater, with a performance enhancement of about 65 %. For the mechanism of acetonitrile removal by this system, we give the responses as: electrically

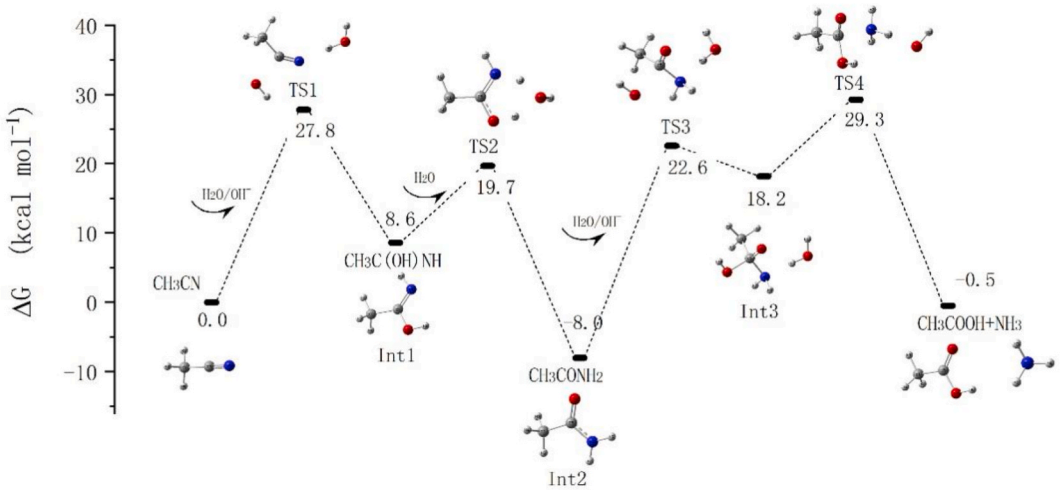

Fig. 10. Optimized model of the key intermediates in the alkaline hydrolysis of acetonitrile in aqueous phase (water) at the B3LYP/6–31++(d, p) level.

Table 5
Main parameters of acetonitrile hydrolysis optimized in aqueous phase at B3LYP/6–31++G(d,p) level [35].

Stationary point	H2–O1	H1–N	C2–N	C2–O1	H3–O2	H3–N	O2–C2
Acetonitrile	0.097	0.208	0.116	0.420			
TS1	0.097	0.298	0.121	0.186			
Int1	0.097	0.311	0.127	0.138			
TS2	0.098	0.227	0.127	0.136			
Int2	0.132	0.133	0.131	0.130			
TS3	0.250	0.101	0.137	0.123			
Int3	0.251	0.102	0.136	0.124	0.099	0.266	0.322
TS4	0.245	0.102	0.160	0.122	0.140	0.114	0.191
Products	0.375	0.102	0.371	0.122	0.428	0.102	0.121

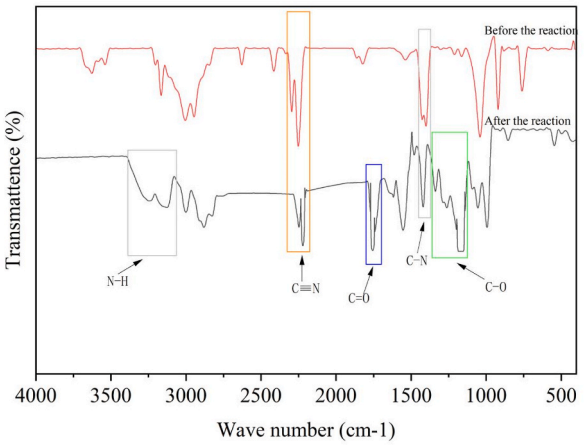

Fig. 11. Infrared spectra of the solutions before and after the reaction.

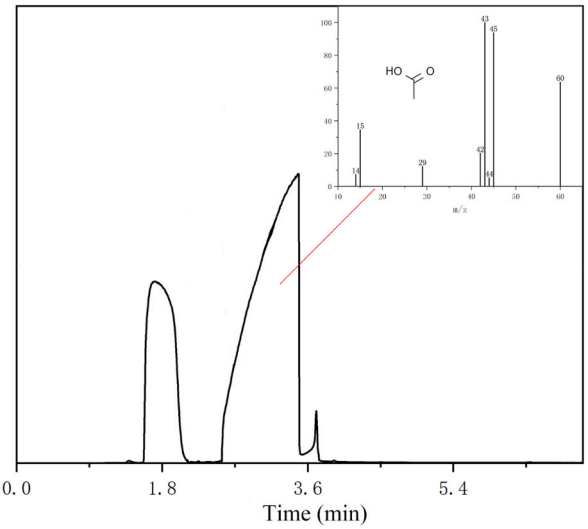

Fig. 12. Infrared spectra of the solutions before and after the reaction.

enhanced adsorption as well as electrocatalytic hydrolysis. The electrically enhanced adsorption is mainly manifested by the polarization of acetonitrile by microelectrode, the oxidation of activated carbon by microelectrode, and the adsorption of acetonitrile by platinum at a certain potential. The electrocatalytic hydrolysis is mainly due to the fact that the acetonitrile molecules occupy the adsorption sites on the surface of the platinum electrode, which leads to the resolution of hydrogen ions and hydroxides, and then the acetonitrile is catalytically hydrolyzed.

Therefore, ME-ACF may be an effective method for the treatment of polar organics.

CRediT authorship contribution statement

Yaping Guo: Writing – review & editing, Resources, Conceptualization. **Shuo Cao:** Writing – review & editing, Writing – original draft, Investigation, Formal analysis. **Sizhou Cheng:** Investigation, Formal analysis. **Xinhua Huang:** Supervision, Formal analysis. **Mengyao Ren:** Supervision.

Declaration of competing interest

The authors declare that they have no known competing financial interests or personal relationships that could have appeared to influence the work reported in this paper.

Acknowledgments

This work is supported by the National Natural Science Foundations of China (Grant No. 51108416) and Zhejiang Provincial Research Foundation for Public Welfare Technology (Grant No. LGF19E080011).

In addition, we would like to thank Tao Wen for his help with the experiments as well as the writing of the paper.

References

[1] V. Jiménez, P. Sánchez, A. Romero, Materials for activated carbon fiber synthesis, in: Activated Carbon Fiber and Textiles, Elsevier, 2017, pp. 21–38, https://doi.org/10.1016/B978-0-08-100660-3.00002-X.
[2] G. Özsin, A.E. Pütün, K. Nakabayashi, J. Miyawaki, S.-H. Yoon, Environmental-friendly production of carbon fiber from isotropic hybrid pitches synthesized from waste biomass and polystyrene with ethylene bottom oil, J. Clean. Prod. 239 (2019), 118025, https://doi.org/10.1016/j.jclepro.2019.118025.
[3] J. Andrews, R. Ojha, S.M. Rezaei Niya, S. Seibt, Electrochemical storage reactions of hydrogen in activated carbon from phenolic resin, Catal. Today 397–399 (2022) 155–164, https://doi.org/10.1016/j.cattod.2021.11.015.
[4] Y. Yue, Y. Wang, C. Qu, X. Xu, Modification of polyacrylonitrile-based activated carbon fibers and their p-nitrophenol adsorption and degradation properties, J. Environ. Chem. Eng. 9 (4) (2021), 105390, https://doi.org/10.1016/j.jece.2021.105390.
[5] U. V C, S. K, K. B R, S. G, R. H, Characterization of untreated and alkali treated Areca catechu fibre through eco-friendly composite plates, Mater. Today: Proc. 52 (2022) 1108–1112, https://doi.org/10.1016/j.matpr.2021.11.004.
[6] J. Pullas Navarrete, E. de la Torre, Preparation of activated carbon fibers (ACF) impregnated with metallic silver particles from cotton-woven wastes and its performance as an antibacterial agent, Mater. Today Commun. 33 (2022), 104598, https://doi.org/10.1016/J.MTCOMM.2022.104598.
[7] K. Hina, H. Zou, W. Qian, D. Zuo, C. Yi, Preparation and performance comparison of cellulose-based activated carbon fibres, Cellulose 25 (1) (2018) 607–617, https://doi.org/10.1007/s10570-017-1560-y.
[8] M. Vijayakumar, R. Santhosh, J. Adduru, T.N. Rao, M. Karthik, Activated carbon fibres as high-performance supercapacitor electrodes with commercial level mass loading, Carbon 140 (2018) 465–476, https://doi.org/10.1016/j.carbon.2018.08.052.
[9] Y. Ge, I. Akpinar, Z. Li, S. Liu, J. Hua, W. Li, T. Zhao, X. Hu, Porous structured cotton based ACF for the adsorption of benzen, Chemosphere 282 (2021), 131110, https://doi.org/10.1016/j.chemosphere.2021.131110.
[10] Z. Zhu, Z. Huang, W. Huang, H. Wen, J. Zhang, P. Wang, Y. Peng, C. Liu, Polymer brush-grafted cotton fiber for the efficient removal of aromatic halogenated disinfection by-products in drinking water, J. Colloid Interface Sci. 597 (2021) 66–74, https://doi.org/10.1016/J.JCIS.2021.03.084.
[11] A. Hashem, C.O. Aniagor, M.F. Nasr, A. Abou-Okeil, Efficacy of treated sodium alginate and activated carbon fibre for Pb(II) adsorption, Int. J. Biol. Macromol. 176 (2021) 201–216, https://doi.org/10.1016/J.IJBIOMAC.2021.02.067.
[12] M. Luo, J. Chen, Q. Li, Y. Wang, Cotton-Based activated carbon fiber with high specific surface area prepared by low-temperature hydrothermal carbonization with urea enhancement, Ind. Eng. Chem. Res. 62 (22) (2023) 8744–8753, https://doi.org/10.1021/acs.iecr.3c00807.
[13] R. Muhammad, Y.C. Nah, H. Oh, Spider silk-derived nanoporous activated carbon fiber for CO2capture and CH4and H2storage, J. CO2 Util. 69 (2023), https://doi.org/10.1016/j.jcou.2023.102401.
[14] Y. Teng, J. Zhu, S. Xiao, Z. Ma, T. Huang, Z. Liu, Y. Xu, Exploring chitosan-loaded activated carbon fiber for the enhanced adsorption of Pb (II)-EDTA complex from electroplating wastewater in batch and continuous processes, Separ. Purif. Technol. 299 (2022), 121659, https://doi.org/10.1016/J.SEPPUR.2022.121659.
[15] S. Tian, Y. Tu, J. Chen, G. Shao, Z. Zhou, Z. Ren, Persulfate enhanced electrochemical oxidation of phenol with CuFe2O4/ACF (activated carbon fibers) cathode, Separ. Purif. Technol. 279 (2021), 119727, https://doi.org/10.1016/j.seppur.2021.119727.
[16] Y. Bi, E. Sun, S. Zhang, F. Du, H. Wei, F. Liu, C. Zhao, Synergistic effect of adsorption and photocatalysis for the degradation of toluene by TiO2 loaded on ACF modified by Zn(CH3COO)2, Environ. Sci. Pollut. Control Ser. 28 (40) (2021) 57398–57411, https://doi.org/10.1007/s11356-021-14539-5.
[17] A. Lissaneddine, M.-N. Pons, F. Aziz, N. Ouazzani, L. Mandi, E. Mousset, Electrosorption of phenolic compounds from olive mill wastewater: mass transport consideration under a transient regime through an alginate-activated carbon fixed-bed electrode, J. Hazard Mater. 430 (2022), 128480, https://doi.org/10.1016/j.jhazmat.2022.128480.
[18] X. Mei, Y. Ding, P. Li, L. Xu, Y. Wang, Z. Guo, W. Shen, Y. Yang, Y. Wang, Y. Xiao, X. Yang, Y. Liu, Y. Shen, Y. Wu, C. Jiang, C. Xue, A novel system for zero-discharge treatment of high-salinity acetonitrile-containing wastewater: combination of pervaporation with a membrane-aerated bioreactor, Chem. Eng. J. 384 (2020), 123338, https://doi.org/10.1016/j.cej.2019.123338.
[19] P. Kunlasubpreedee, C. Visvanathan, Performance evaluation of membrane-aerated biofilm reactor for acetonitrile wastewater treatment, J. Environ. Eng. 146 (7) (2020), https://doi.org/10.1061/(ASCE)EE.1943-7870.0001706.
[20] N. Phosirikul, C. Visvanathan, E.R. Rene, Removal of gas phase methanol and acetonitrile mixture in an air membrane bioreactor (aMBR) under steady and transient-state operations, Bioresour. Technol. 376 (2023), 128824, https://doi.org/10.1016/j.biortech.2023.128824.
[21] C. Urita, K. Urita, T. Araki, K. Horio, M. Yoshida, I. Moriguchi, New insights into the heat of adsorption of water, acetonitrile, and n-hexane in porous carbon with oxygen functional groups, J. Colloid Interface Sci. 552 (2019) 412–417, https://doi.org/10.1016/j.jcis.2019.05.090.
[22] J.H. Tsai, H.M. Chiang, G.Y. Huang, H.L. Chiang, Adsorption characteristics of acetone, chloroform and acetonitrile on sludge-derived adsorbent, commercial granular activated carbon and activated carbon fibers, J. Hazard Mater. 154 (1–3) (2008) 1183–1191, https://doi.org/10.1016/j.jhazmat.2007.11.065.
[23] K.Y. Foo, B.H. Hameed, A short review of activated carbon assisted electrosorption process: an overview, current stage and future prospects, J. Hazard Mater. 170 (2–3) (2009) 552–559, https://doi.org/10.1016/j.jhazmat.2009.05.057.
[24] S. Furmaniak, Influence of activated carbon porosity and surface oxygen functionalities' presence on adsorption of acetonitrile as a simple polar volatile organic compound, Environ. Technol. 36 (15) (2015) 1984–1999, https://doi.org/10.1080/09593330.2015.1018843.
[25] C. Urita, K. Urita, T. Araki, K. Horio, M. Yoshida, I. Moriguchi, New insights into the heat of adsorption of water, acetonitrile, and n-hexane in porous carbon with oxygen functional groups, J. Colloid Interface Sci. 552 (2019) 412–417, https://doi.org/10.1016/j.jcis.2019.05.090.
[26] J. Zhou, Y. Zhang, M. Balda, V. Presser, F.-D. Kopinke, A. Georgi, Electro-assisted removal of polar and ionic organic compounds from water using activated carbon felts, Chem. Eng. J. 433 (2022), 133544, https://doi.org/10.1016/j.cej.2021.133544.

[27] Gracy Elias, Earl D. Mattson, Jessica E. Little, A HPLC method for the quantification of butyramide and acetamide at ppb levels in hydrogeothermal waters, Anal. Methods 4 (2) (2012) 530–533.
[28] M.T.M. Koper, Blank voltammetry of hexagonal surfaces of Pt-group metal electrodes: comparison to density functional theory calculations and ultra-high vacuum experiments on water dissociation, Electrochim. Acta 56 (28) (2011) 10645–10651, https://doi.org/10.1016/j.electacta.2011.02.001.
[29] K. Ojha, N. Arulmozhi, D. Aranzales, M.T.M. Koper, Double layer at the Pt (111)–aqueous electrolyte interface: potential of zero charge and anomalous gouy–chapman screening, Angew. Chem. Int. Ed. 59 (2) (2020) 711–715, https://doi.org/10.1002/anie.201911929.
[30] A.V. Rudnev, E.B. Molodkina, A.I. Danilov, Yu M. Polukarov, A. Berna, J.M. Feliu, Adsorption behavior of acetonitrile on platinum and gold electrodes of various structures in solution of 0.5M H2SO4, Electrochim. Acta 54 (14) (2009) 3692–3699, https://doi.org/10.1016/j.electacta.2009.01.047.
[31] Jinggang Lan, Vladimir V. Rybkin, Iannuzzi Marcella, Ionization of water as an effect of quantum delocalization at aqueous electrode interfaces." the journal of physical chemistry letters, Frisch, M. J., G. W. Trucks, and H. B. Schlegel. "Gaussian 09, Revision D. 01, Gaussian, Inc., Wallingford, CT, 2009 11 (9) (2020) 3724–3730;
(b) A.D. Becke, Phys. Rev. A 38 (1988) 3098–3100.
[32] Joseph W. Ochterski, George A. Petersson, John A. Montgomery Jr., A complete basis set model chemistry. V. Extensions to six or more heavy atoms, The Journal of chemical physics 104 (7) (1996) 2598–2619.
[33] Andrea Grisafi, et al., Symmetry-adapted machine learning for tensorial properties of atomistic systems, Phys. Rev. Lett. 120 (3) (2018), 036002.
[34] M.J. Frisch, et al., Gaussian, Inc., Wallingford CT, 2016." Gaussian09, Revision D 1 (2016).
[35] Fenji Li, et al., Theoretical study on the hydrolysis mechanism of acetonitrile and its chlorinated derivatives, Journal of Yunnan University for Nationalities (Natural Sciences Edition) 27 (5) (2018) 382–388.